Distribution of Mitochondrial NADH Fluorescence Lifetimes: Steady-State Kinetics of Matrix NADH Interactions

Ksenia Blinova,*,‡ Stefanie Carroll,‡ Salil Bose,‡,§ Aleksandr V. Smirnov,|| John J. Harvey,||,⊥ Jay R. Knutson,|| and Robert S. Balaban‡

Laboratory of Cardiac Energetics and Laboratory of Biophysical Chemistry, National Heart, Lung, and Blood Institute, National Institutes of Health, Bethesda, Maryland 20892

Received July 13, 2004; Revised Manuscript Received November 2, 2004

ABSTRACT: The lifetimes of fluorescent components of matrix NADH in isolated porcine heart mitochondria were investigated using time-resolved fluorescence spectroscopy. Three distinct lifetimes of fluorescence were resolved: 0.4 (63%), 1.8 (30%), and 5.7 (7%) ns (% total NADH). The 0.4 ns lifetime and the emission wavelength of the short component were consistent with free NADH. In addition to their longer lifetimes, the remaining pools also had a blue-shifted emission spectrum consistent with immobilized NADH. On the basis of emission frequency and lifetime data, the immobilized pools contributed >80% of NADH fluorescence. The steady-state kinetics of NADH entering the immobilized pools was measured in intact mitochondria and in isolated mitochondrial membranes. The apparent binding constants (K_Ds) for NADH in intact mitochondria, 2.8 mM (1.9 ns pool) and >3 mM (5.7 ns pool), were on the order of the estimated matrix [NADH] (~3.5 mM). The affinities and fluorescence lifetimes resulted in an essentially linear relationship between matrix [NADH] and NADH fluorescence intensity. Mitochondrial membranes had shorter emission lifetimes in the immobilized poo1s [1 ns (34%) and 4.1 ns (8%)] with much higher apparent K_Ds of 100 μM and 20 μM, respectively. The source of the stronger NADH binding affinity in membranes is unknown but could be related to high order structure or other cofactors that are diluted out in the membrane preparation. In both preparations, the rate of NADH oxidation was proportional to the amount of NADH in the long lifetime pools, suggesting that a significant fraction of the bound NADH might be associated with oxidative phosphorylation, potentially in complex 1.

Mitochondria participate in a number of metabolic reactions, but their principal biological function is energy conversion. Adenosine triphosphate (ATP)[1] produced by mitochondrial oxidative phosphorylation is the primary molecular source of energy for the functional activities of mammalian cells. The phosphorylation of adenosine diphosphate (ADP) in oxidative phosphorylation is coupled to the oxidation of the principal electron donor, reduced nicotinamide adenine dinucleotide (NADH). Thus, insight into the compartmentation and protein interactions of mitochondrial NADH is fundamental to the understanding of overall cellular energy metabolism.

As pioneered by Chance and colleagues (*1*), the intrinsic fluorescence of nicotinamide adenine dinucleotide phosphate, reduced [NAD(P)H], has been an extremely useful tool in the noninvasive monitoring of tissue energy metabolism. In heart tissue, mitochondrial NAD(P)H levels are much lower than NADH; thus the fluorescence signal from heart mitochondria can essentially be considered to be from NADH alone (*2*, *3*). Early studies appreciated that, in contrast to absorption, NAD(P)H fluorescence lifetime and emission spectra strongly depend on the microenvironment (*4*−*7*). This led to the observation that the fluorescence enhancement ratio, i.e., the amount of fluorescence per mole of NADH, is increased in some binding environments (*6*, *7*). The dependence of NAD(P)H fluorescence on the microenvironment makes the interpretation of these signals in intact tissues complicated. To evaluate the contribution of different compartments to the overall cellular NAD(P)H fluorescence signal, several different approaches have been taken, including spectral analysis (*4*, *5*, *7*, *8*), microimaging (*2*, *9*, *10*), carbon substrate dependence (*2*, *11*, *12*), and fluorescence lifetime measurements (*13*, *14*).

* Address correspondence and reprint requests to this author. Tel: 301-594-8743. Fax: 301-402-2389. E-mail: blinovak@nhlbi.nih.gov.

‡ Laboratory of Cardiac Energetics, National Heart, Lung, and Blood Institute.

§ Current address: School of Biological Sciences, Nanyang Technological University, Singapore.

|| Laboratory of Biophysical Chemistry, National Heart, Lung, and Blood Institute.

⊥ Current address: Excimus Biotech, Inc., Baltimore, MD 21202.

[1] Abbreviations: NAD, nicotinamide adenine dinucleotide; NADH, nicotinamide adenine dinucleotide, reduced; NAD^+, nicotinamide adenine dinucleotide, oxidized; NAD(P)H, nicotinamide adenine dinucleotide phosphate, reduced; FAD, flavin adenine dinucleotide; GM, potassium glutamate and potassium malate; FCCP, carbonyl cyanide 4-(trifluoromethoxy)phenylhydrazone; ATP, adenosine triphosphate; ADP, adenosine diphosphate; TMPD, *N*,*N*,*N*′,*N*′-tetramethyl-*p*-phenylenediamine; TCSPC, time-correlated single-photon counting technique; DAS, decay-associated spectra; $\Delta\Psi$, membrane potential; CHAPS, 3-[(3-cholamidopropyl)dimethylammonio]-1-propanesulfonate; FRET, Förster resonance energy transfer; EGTA, ethylene glycol bis-(2-aminoethyl ether)-*N*,*N*,*N*′,*N*′-tetraacetic acid; K_2EDTA, dipotassium ethylenediaminetetraacetate; HEPES, *N*-(2-hydroxyethyl)piperazine-*N*′-2-ethanesulfonic acid; P_i, inorganic phosphate; TPP^+, tetraphenylphosphonium ion; K_D, dissociation constant.

10.1021/bi0485124
Published on Web 01/25/2005

The emission spectra of most tissues (*2*, *5*, *15*) have been demonstrated to be blue shifted by 10−15 nm as compared to free NAD(P)H in solution, suggesting that the fluorescence emission is dominated by the NAD(P)H pools which are immobilized. To our knowledge, no attempt has been made to spectrally resolve different NAD(P)H pools in intact systems.

Another complication has been the need to discern the relative contributions of cytosolic and mitochondrial NAD(P)H pools to the emission characteristics. Aside from physical separation, two approaches have been used to isolate the signals from these pools. With the use of selective metabolic substrates, the redox state of the cytosol has been manipulated (*12*, *16*). Another approach was to directly image mitochondrial and cytosolic NAD(P)H using microfluorescence techniques (*2*, *9*, *17*, *18*).

Of all these methods, the fluorescence lifetime provides the most quantitative measure of different NAD(P)H fluorescence pools contributing to fluorescence enhancement in complicated biological samples. In intact cells and mitochondria, three fluorescence lifetime pools are generally observed: the free$_m$ NAD(P)H pool (with a lifetime of ~0.2−0.4 ns), an intermediate$_m$ pool (1−2 ns), and a long$_m$ lifetime pool (3−8 ns) (*13*, *14*). The m subscript refers to mitochondrial NADH pools. The intermediate$_m$ and long$_m$ lifetime pools were ascribed to protein binding of NAD(P)H. The relative sizes of these pools also suggested that the majority of the steady-state fluorescence collected from these systems is dominated by this immobilized pool, in agreement with the earlier emission spectral analysis. There is much less information available on the dynamic redistribution of NAD(P)H pools during physiological perturbations. In liver mitochondria, Wakita et al. (*13*) reported that the mean lifetime of NAD(P)H fluorescence was constant at 2.8 ± 0.05 ns during numerous perturbations, including active ATP production (state 3), resting (state 4), and uncoupled conditions. This occurred despite the fact that the matrix [NAD(P)H] and NAD(P)H turnover were modified over nearly the full physiological range. These data suggested that the relative fraction of binding was constant despite large changes in matrix NAD(P)H concentration or flux. The mechanism(s) for maintaining this constant fraction of immobilized NAD(P)H is (are) unknown.

Some of the binding sites within the mitochondrial matrix are malate dehydrogenase (*19*, *20*), succinate dehydrogenase (*21*), and citrate synthase (*22*). The fluorescence lifetime and emission shift effects are themselves nonspecific (*7*), and it is likely that many interaction sites exist in the matrix environment. The overall steady-state kinetics for [NAD(P)H] binding in the mitochondrial matrix has not been established.

The purpose of the current study was to characterize both the fluorescence emission spectra and lifetime of cardiac mitochondrial NADH ([NADPH] is assumed to be negligible), to determine the steady-state matrix binding kinetics for NADH as compared to the kinetics of NADH oxidation by the cytochrome chain, and to establish the relationship between the total matrix NADH/NAD^+ and the bound NADH/NAD^+ pool under various conditions.

MATERIALS AND METHODS

Three buffers were employed as media for intact mitochondria and mitochondrial membranes: buffer A contained 137 mM KCl, 10 mM *N*-(2-hydroxyethyl)piperazine-*N*′-2-ethanesulfonic acid (HEPES), 2.5 mM $MgCl_2$, and 0.5 mM K_2EDTA; buffer B contained 125.0 mM KCl, 20.0 mM HEPES, 1.0 mM EGTA, 1.0 mM K_2EDTA, and 5.0 mM $MgCl_2$; and buffer C contained 137 mM KCl, 20 mM HEPES, and 1.0 mM EGTA. The pH of these buffers was adjusted to 7.1 with KOH.

Isolation of Heart Mitochondria. Mitochondria were isolated from pig hearts, cold perfused in situ to minimize warm hypoxic damage, as described by Territo et al. (*23*). Mitochondria were suspended in buffer A. Potassium glutamate and potassium malate (GM) were added when a reducing equivalent source was required. The respiratory control ratio (the ratio of the rates of oxygen consumption in the presence and in the absence of ADP) of each preparation was measured, and for all experiments the initial respiratory control ratios were >10. Since the concentration of NADPH in heart mitochondria is much lower than NADH, it is assumed that the majority of the blue fluorescence originates from NADH. The cytochrome *a* (cyt_a) content was determined spectrophotometrically in Triton X-100 extracts as previously described (*24*).

Pulverized Mitochondria. Mitochondria with exposed matrix elements were obtained by freezing the mitochondrial suspension (buffer A) in liquid nitrogen and pulverizing the frozen pellet using a tissue Bessman pulverizer (BioSpec Products Inc., Bartlesville, OK). The thawing and freeze−pulverizing cycle was repeated two times. The pulverized preparation showed rapid respiration in the presence of exogenous NADH (see Results section). No enhancement of respiration occurred with an uncoupler (FCCP) or with ADP and P_i. These data are consistent with nearly complete opening of the matrix elements in this preparation.

Oxygen Consumption, Mitochondrial Membrane Potential, and NADH Emission. The rate of oxygen consumption from a gastight water-jacketed stirred chamber was measured using an YSI Clark electrode (Yellow Springs, OH). The specific chamber used is the same as previously reported (*25*). Data were digitized and stored in a custom-built analog-to-digital conversion system. Only the initial rate of oxygen consumption following the addition of NADH was analyzed since the consumption of NADH could be quite significant and might alter the bath [NADH]. The linear increase only occurred over the first 30 s of the tracing when very low concentrations of NADH were utilized. The incubation was performed at 25 °C in buffer C to match the lifetime data which were collected routinely at 25 °C. Carbon substrates that could generate NADH were not added when evaluating the oxidation of NADH in pulverized preparations while any carbon substrates intrinsic to the preparation were used up in the equilibration period of these experiments.

Fluorescence Spectra. Spectra were measured using two approaches. For simple standardization studies standard 1 cm quartz cuvettes were used in a luminescence spectrometer (PerkinElmer Life Sciences LS55 Boston, MA) NADH fluoresence spectra were obtained as difference spectra calculated by subtraction of mitochondrial suspension fluorescence spectra in the fully oxidized conditions (in presence

of ADP, P_i, FCCP and absence of GM) from the spectra obtained in reduced conditions. This approach minimized but did not eliminate inner filter effects. In the second approach NADH fluoresence spectra were collected in diluted mitochondrial suspensions and in small quartz cuvettes (3×3 mm, Spectrocell Inc., Oreland, PA) to reduce absorbance and emitted light pathlength. The total volume of the sample was only 50 μL. Adequate emission signal to noise was obtained using a high power pulsed laser at 355 nm (Continuum Surelite 1; Continuum, Santa Clara, CA, peak power is 80 mW over ~0.2 cm^2) as the excitation source. Since the laser power was strong enough to photolyze NADH (*3*), only one NADH spectrum was collected for analysis during a single laser pulse on the sample. NADH fluorescence was detected at 90 °C to the excitation beam using a fiber-optic-based rapid-scan spectrofluorometer (*27*). As an additional control, emission spectra were collected over a range of mitochondrial concentrations from 0.5−2 mmol cyt_a/mL in buffer B which demonstrated that the spectral shape was unaffected by the concentration of mitochondria under these conditions (not shown), and was consistent with the elimination of inner filter effects.

Absorption Spectra. To minimize the mitochondrial light scattering effects on the measurement of the relative absorption spectra, an integrating sphere was used that allowed the collection of scattered photons (PerkinElmer Life Sciences Model Lambda 800, Boston, MA) (*28*). Quantitative analysis was performed by calculating the ΔA of mitochondrial NADH peak absorbance (at 340 nm) in the reduced state versus fully oxidized mitochondria (in the presence of ADP, P_i, and no GM). The percent of reduced nucleotide was calculated as

$$\%_{red} = \frac{A^{340} - A^{340}_{\text{fully oxidized}}}{A^{340}_{\text{fully reduced}} - A^{340}_{\text{fully oxidized}}}$$

where A^{340}, $A^{340}_{\text{fully reduced}}$, and $A^{340}_{\text{fully oxidized}}$ are the relative absorption at 340 nm of the sample, of fully oxidized mitochondria (ADP, P_i, no GM, FCCP), and of fully reduced mitochondria (GM, anoxia), respectively. The path length was not determined in these studies and is assumed to be constant in this highly scattering media.

Fluorescence Decay Measurement. Time-resolved fluorescence measurements were performed by the time-correlated single-photon counting technique (TCSPC) (*29*) with the following modifications: samples were excited at 335 nm using a synchronously pumped, frequency doubled, cavity dumped dye laser (repetition rate 4 MHz, pulse width 2 ps, average UV power <200 μW). The channel width was 36 ps, and data were collected in 512 channels. Fluorescence decays were collected under "magic angle" polarization conditions (*30*) with the emission monochromator set at 440 nm. Assuming that fluorescence decay follows a multiexponential law, the total intensity may be calculated as

$$I(t,\lambda) = \sum_i^n \alpha_i(\lambda) e^{-t/\tau_i} + \alpha_s(\lambda)\delta(t)$$

For each sample, the relative amplitudes α_i and decay constants τ_i were the recovered parameters. An independent parameter α_s represents the sum of Rayleigh and Raman scattering. Since the short lifetime component of NADH is due to self-quenching of the nicotinamide by the adenine ring (*31*), the radiative rates of free and bound species should be nearly the same. As will be discussed below, the decay-associated spectra (DAS) for free and bound species are quite similar, with <25 nm blue shift upon binding. The radiative rate is dependent upon overlap between excited and ground state envelopes, so there may be a slightly weaker radiative rate for the red-shifted (free) species (*32*). Nevertheless, the ratios of the preexponential terms, α_i, are a good proxy for the concentration ratios. The relative concentration of [NADH-free]/[NADH-total] was therefore calculated as $\alpha_{short}/\sum\alpha_i$, where short implies all species with τ ~0.2−0.5 ns. In all time-resolved fluorescence experiments, the reference lamp profile and the color shift used for convolution analysis were tested with a monoexponential standard (9-anthracenecarbonitrile in methanol with a fluorescence lifetime τ = 12 ns). The convolution was compared with the experimental decay by nonlinear least-squares analysis. The best fit between the theoretical curve and the data was evaluated from the plot of weighted residuals, the autocorrelation function of the weighted residuals, and the reduced χ^2 value. Estimation of error in the fitting parameters was done using the "χ^2_R-surface" plane method. The uncertainty in the recovered variable was calculated on the basis of a 90% confidence interval, which usually corresponds to a 10% increase in the χ^2_R minimum value.

Decay-Associated Spectra (DAS). DAS were obtained from a global fit of the decay profiles collected at different wavelengths with the common lifetimes τ_l-linked across the data set while optimizing the amplitudes α_i for each decay (*33*).

RESULTS

NADH Fluorescence Spectra. Fluorescence spectra of NADH from intact mitochondria, pulverized mitochondria, and free NADH in solution are presented in Figure 1. The fluorescence maximum of NADH in intact mitochondria is blue shifted ~15 nm compared to free NADH fluorescence, which is consistent with the suggestion that the bound form of NADH is the major contributor to emission (*5*, *7*). Surprisingly, the emission spectrum from the pulverized mitochondria was essentially the same as that of intact mitochondria. With the opening of the matrix space by the pulverization process, the free matrix [NADH] should be significantly reduced. Disrupting a mitochondrial suspension of 1 nmol of cyt_a/mL should dilute the matrix NADH by ~500-fold (assuming ~2 μL of matrix volume/nmol of cyt_a). In addition to the functional studies showing no oxidative phosphorylation coupled electron flow and direct oxidation of NADH (see Materials and Methods), we confirmed that matrix NADH was exposed by removing NADH from the pellet by washing the pulverized preparation several times by centrifugation (16000*g*, 10 min). Despite the large dilution, even in the initial opening of the matrix, the pulverized mitochondrial NADH fluorescence spectra were essentially identical to those of intact mitochondria, suggesting that the bound fraction of NADH still dominated the emission spectra. These results suggest a very high affinity for NADH binding in the matrix. Similar effects were observed when Triton X-100 (1%), CHAPS, or octyl

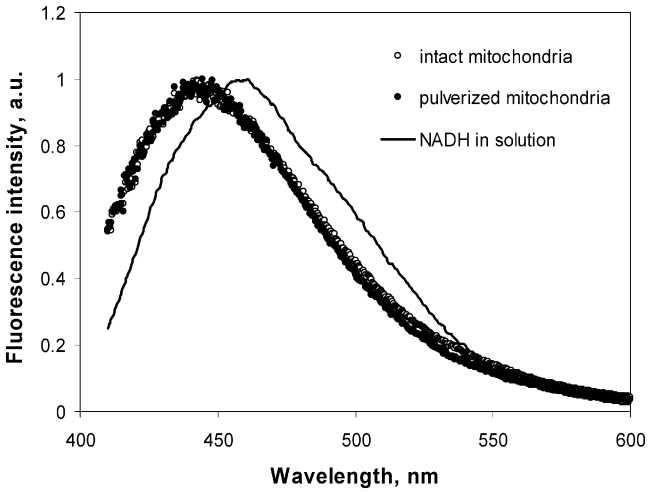

FIGURE 1: Normalized fluorescence spectra of NADH in intact mitochondria, pulverized mitochondria, and free NADH in buffer B. The concentration of intact mitochondria and pulverized mitochondria was 1 nmol of cyt_a/mL while the free [NADH] = 100 μM. Fluorescence spectra were measured using single laser pulse for excitation in a small quartz cuvette to diminish the scattering effect (see Materials and Methods). Fluorescence spectra of intact mitochondria are represented by open circles, spectra of pulverized mitochondria by filled circles, and spectra of the solution of NADH by a solid line.

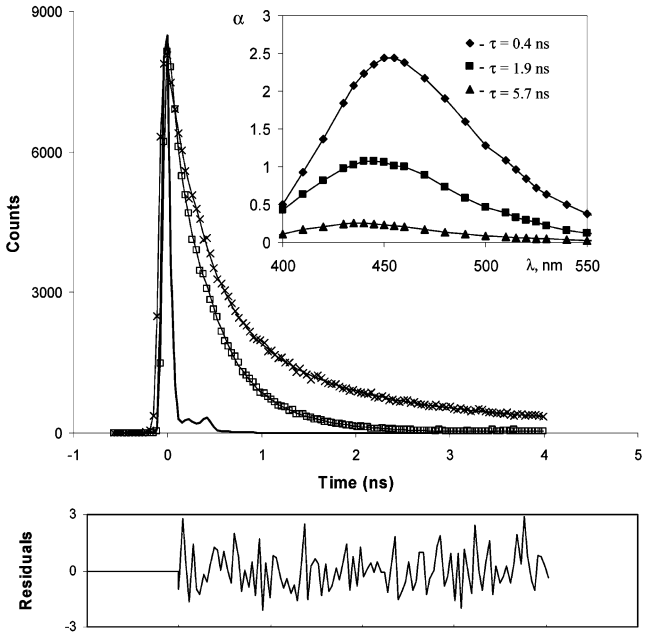

FIGURE 2: Time-resolved fluorescence decay of curves of free NADH in solution (white squares), intact mitochondria (crosses), and the instrument response function (black solid line). The solid lines drawn through the decay curves show a three-exponential fit. The intact mitochondria were incubated in buffer B in the presence of 5 mM GM. The NADH data of the pulverized mitochondria were collected in the presence of 10 mM CN and 5 mM GM to maximize [NADH] and prevent its oxidation. The lower curve shows the typical random residual distribution of the fit for pulverized mitochondria. The insert shows the DAS for three lifetime pools of intact mitochondria under identical conditions used for the lifetime measurements alone.

β-glucoside were used to disrupt the matrix compartment (not shown).

Mitochondrial NADH Fluorescence Lifetimes. Examples of NADH fluorescence decay curves for free NADH in solution and in nearly fully reduced (State 4) mitochondria are shown in Figure 2. The decay curves fit satisfactorily with three exponentials. The insert in Figure 2 shows the DAS from intact mitochondria under the same conditions. The DAS of $long_m$ and $intermediate_m$ lifetime NADH components are blue shifted by ~20 nm relative to the free or short lifetime pool, which is consistent with the steady-state spectra. The individual lifetimes and the average lifetimes of NADH fluorescence for intact and pulverized mitochondria, the calculated molar fraction of each lifetime pool, and the contribution of each lifetime pool to the fluorescence intensity are presented in Table 1.

The estimated lifetimes in intact mitochondria are 0.44 ($free_m$), 1.88 ($intermediate_m$), and 5.7 ($long_m$) ns, values similar to those reported earlier (*13*). The largest NADH pool was the $free_m$ pool at ~60% followed by the $intermediate_m$ pool (at 30%) and the $long_m$ pool (7%) of NADH. Estimation of the relative contribution (f_i) of each component to the total fluorescence emission shows that the blue-shifted $intermediate_m$ and $long_m$ pools together contribute ~80% of the emitted light. A simulated steady-state emission spectrum from the lifetime data has been constructed using the DAS spectra for each component and the $\alpha\tau$ (amplitude × lifetime) values. The constructed spectrum is compared with the directly measured experimental spectrum in Figure 3. The excellent correlation suggests that the steady-state spectrum can be adequately described by these lifetime components.

As in the case of the intact system, the pulverized preparation also shows three NADH pools with emission lifetimes of 0.29 ($free_p$), 1.0 ($intermediate_p$), and 4.1 ($long_p$) ns, but these are somewhat shorter than those found in intact mitochondria (the p subscript indicates NADH pools in the pulverized preparation). The relative proportions of the components were essentially the same as in the intact mitochondria; however, the $intermediate_p$ plus the $long_p$ pools still dominated the overall emission to the same extent (~80%). These data suggest that NADH remains significantly immobilized in the pulverized preparation but that the pulverization process has modified the actual molecular environment. Since the pulverization process causes a rather drastic change in quaternary structure, the modest change in the lifetimes is not that surprising. In any event, the fact that a significant fraction of NADH remains in the intermediate to long pools in the pulverized preparation suggests that the affinity of NADH for binding is very high under these conditions.

To estimate the binding affinity for NADH in mitochondrial membranes, pulverized mitochondria (0.53 nmol of cyt_a/mL of assay mixture) were titrated with free exogenous NADH. To avoid oxidation of the NADH by the electron transfer chain, 10 mM cyanide was added to the preparation, resulting in a maximally reduced NADH level with no detectable net oxidation. The initial total [NAD] in the suspension was estimated to be ~3.40 μM, assuming 6.8 nmol of NADH/nmol of cyt_a and a 2 μL matrix volume/nmol of cyt_a (*3*). The total [NADH] in the suspension was varied from 3.40 to 53.4 μM, and the fluorescence lifetime pools were determined. The results are presented in Figure 4.

The $long_p$ and $intermediate_p$ lifetime pools are saturated with increasing total [NADH] while the free pool continued to increase in this limited range. Saturation of the long-

Table 1: Summary of TCSPC Data for Intact State 4 and Cyanide-Treated Pulverized Mitochondria

sample	*N*		free	intermediate	long
intact mitochondria	6	lifetime, ns	0.44 ± 0.02	1.88 ± 0.04	5.68 ± 0.48
		fraction	0.63 ± 0.12	0.30 ± 0.09	0.07 ± 0.03
		fl contribution	0.23 ± 0.08	0.45 ± 0.05	0.32 ± 0.04
		av lifetime, ns		1.24 ± 0.23	
pulverized mitochondria	5	lifetime, ns	0.29 ± 0.04	1.0 ± 0.2	4.1 ± 0.7
		fraction	0.58 ± 0.07	0.34 ± 0.06	0.08 ± 0.01
		fl contribution	0.21 ± 0.06	0.41 ± 0.05	0.38 ± 0.01
		av lifetime, ns		0.82 ± 0.17	

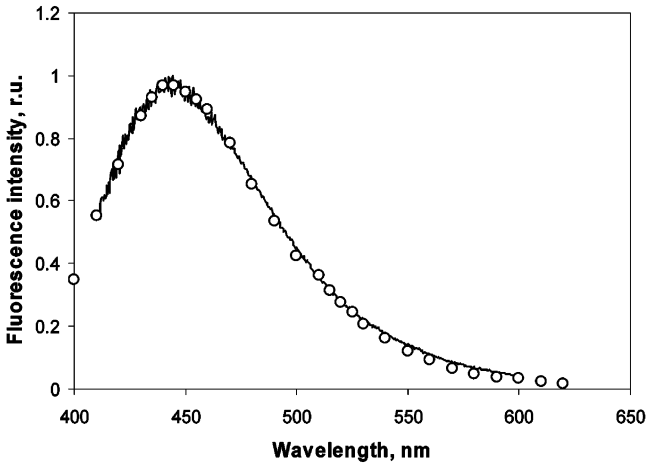

FIGURE 3: Comparison of the calculated NADH fluorescence spectrum from DAS data and the measured NADH fluorescence spectrum in intact mitochondria. The simulated spectrum (open symbols) was constructed by summing the $\alpha\tau$ (amplitude × lifetime) weighted DAS spectra for each lifetime component. The measured NADH spectrum was from a dilute sample of mitochondria (0.50 nmol of cyt$_a$/mL) recorded using a high-power UV laser pulse to minimize inner filter effects (see Materials and Methods).

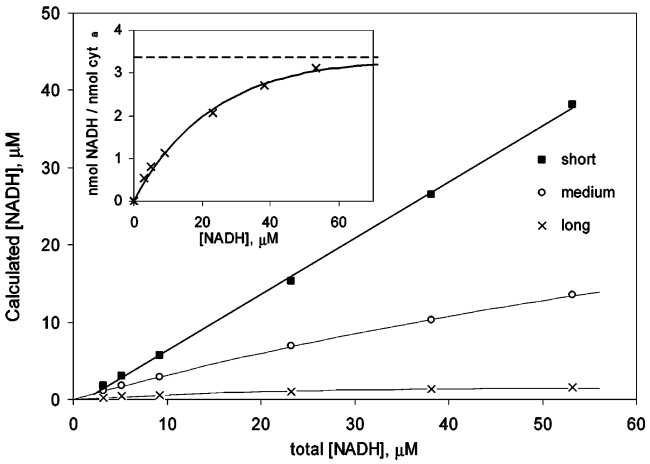

FIGURE 4: Effect of total NADH on NADH distribution in fluorescence lifetime pools in pulverized mitochondria. Pulverized mitochondria (0.53 nmol of cyt$_a$/mL) were titrated with exogenous NADH, and the distribution of NADH in the different lifetime pools was determined. Concentrations of the three NADH lifetime pools, short$_p$ (filled squares), intermediate$_p$ (open circles), and long$_p$ (crosses), are plotted versus total [NADH]. Total [NADH] represents the contributions of both the intrinsic NADH plus the exogenously added NADH. The solid lines are fit with the equation $a(1 - e^{-[NADH]/K_D})$, where a is constant. The insert is the dose response data for the long$_p$ component in an expanded format to illustrate saturation with the calculated long$_p$ NADH concentration converted to nmol of NADH/nmol of cyt$_a$ to estimate the number of binding sites.

lifetime component is more clearly depicted by normalizing NADH to nanomoles of NADH per nanomole of cyt$_a$ (insert). The saturable kinetics for these two pools are characterized by estimating the binding constants (K_D) and the binding capacities (Table 2). The data suggest that the NADH binding sites, under these conditions, have a very high affinity (micromolar) and capacity (~61 nmol of NADH/nmol of cyt$_a$) for NADH, especially when considering that the total matrix [NADH] is only ~3 mM, corresponding to ~7 nmol of NADH/nmol of cyt$_a$ (*3*). These steady-state kinetic data from pulverized mitochondria suggest that essentially all of the NADH should be "bound" in the matrix under normal conditions, which is clearly not the case in intact mitochondria (Table 1), where only ~35% NADH is in a bound state.

We hypothesized that the observed binding of NADH in the pulverized preparation was partially related to the utilization of NADH in electron transfer through the cytochrome chain. To test this hypothesis, the [NADH] dependence of mitochondrial oxygen consumption was determined in the pulverized preparation. The effects of bath oxidation of NADH on the [NADH] was minimized by using low concentrations of pulverized mitochondria (0.1 nmol of cyt$_a$/mL) as well as by considering only the initial rates of oxygen consumption. The oxygen consumption dependence on [NADH] was saturable with a half-maximal value $K_{1/2}$ of 23 mM (Figure 5), which is essentially identical to the K_D of NADH in the long lifetime pool of the same preparation (Table 2). These data suggest that a significant fraction of NADH binding sites might be related to the rate-limiting

Table 2: Summary of Binding Kinetics Data for Intact Mitochondria and Pulverized Mitochondria

		free	intermediate	long
intact mitochondria	τ, ns	0.4	1.9	5.7
	K_D, μM	N/A	2920 ± 240	>3000
	capacity, nmol of NADH/nmol of cyt$_a$	N/A	4.32 ± 0.37	ND
pulverized mitochondria	τ, ns	0.3	1.0	4.1
	K_D, μM	N/A	103 ± 8	24 ± 2
	capacity, nmol of NADH/nmol of cyt$_a$	N/A	61 ± 5	3.4 ± 0.3

steps of NADH oxidation by the cytochrome chain in this uncoupled preparation. It was noted that no inhibition of NADH oxidation was observed at high [NADH] (Figure 5), which is inconsistent with product inhibition by NADH (at these levels) on complex 1 NADH oxidation. Since [NAD^+] is on the same order of magnitude of [NADH] in the matrix for these studies, we further evaluated whether exogenous [NAD^+] had any effect on NADH oxidation. The addition of 2 mM NAD^+ increased the half-maximal value of [NADH]-dependent oxygen consumption to only ~40 mM (Figure 5). Although this increase was significant ($p < 0.05$,

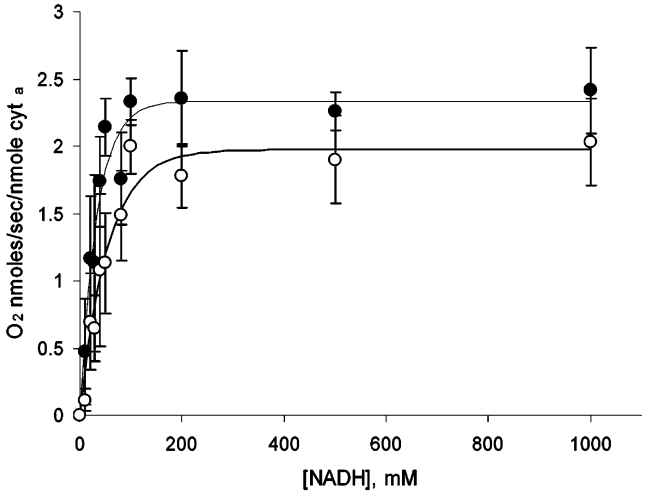

FIGURE 5: Steady-state kinetics of NADH oxidation in pulverized mitochondria. Oxidation of NADH was measured by monitoring the rate of oxygen consumption, as described in Materials and Methods. Only the initial rate of O_2 consumption during the first 30 s following the addition of NADH was analyzed to avoid the consumption of NADH significantly influencing the total bath concentration. Experiments were conducted in buffer C. Closed symbols are for NADH additions alone. The open symbols are in the presence of 2 mM NAD^+ added to buffer C. These are paired experiments from the same sample preparations ($n = 3$). The error bars show the standard errors of mean values. Solid lines are drawn to guide the eye between the two data sets.

$n = 3$), the overall difference was less than 2-fold, which indicates that there was minimal inhibition of NADH oxidation by high levels of NAD^+.

In intact mitochondria, we do not have direct access to manipulate [NADH] or [NAD^+] independently. The total NAD pool in the matrix is constant due to its compartmentation in the matrix. Physiological perturbations are usually associated with changes in the NADH/NAD^+ ratio and not by changes in [NADH] or [NAD^+] alone. Thus, we varied the NADH/NAD^+ ratio in intact mitochondria to determine the effect of this ratio on the distribution of NADH within the different lifetime pools, as well as to estimate the NADH matrix binding affinity to compare to the pulverized preparation. In addition, this protocol permits us to evaluate whether the overall NADH fluorescence intensity is proportional to the [NADH] in the matrix, for future noninvasive monitoring needs. The NADH/NAD^+ ratio was systematically varied by altering the GM concentration. Using this approach, matrix [NADH] could be varied from ~1 to 3.4 mM. Below 1 mM, the contamination from FAD fluorescence becomes more significant and interferes with the lifetime measurements (*34*). The total NADH concentration in these studies was estimated from relative absorption measurements, as described by Bose et al. (*28*). The results of this study are presented in Figure 6 and in Table 2. The intermediate$_m$ pool saturated with increasing total [NADH] as did the intermediate$_p$ pool (Figure 4). The K_D value for intermediate$_m$ binding was, however, very high, at 2.9 ± 0.2 mM. In contrast, both the free$_m$ and long$_m$ pools increased linearly with total [NADH]. The apparent K_D value for long$_m$ binding in intact mitochondria exceeds 3 mM, in sharp contrast to the pulverized preparation with K_D values in the micromolar range. These data indicate either that the binding of NADH is severely inhibited in intact mitochondria when compared to the pulverized preparation or that the variation in the

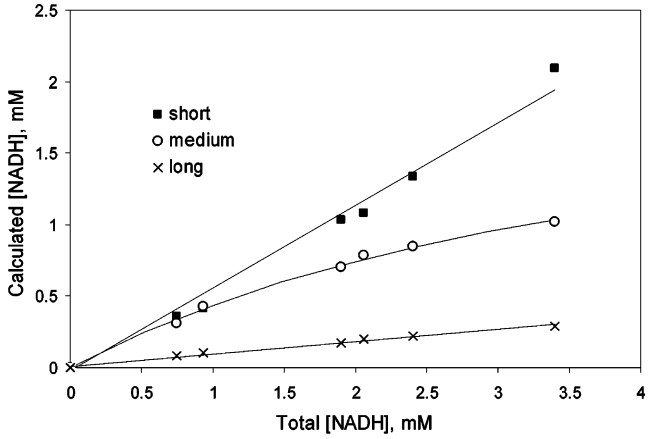

FIGURE 6: Effect of matrix [NADH] on the distribution of NADH in fluorescence lifetime pools. The concentration of NADH was adjusted by varying the concentration of glutamate and malate in the incubation medium. The short$_m$ (filled squares), intermediate$_m$ (open circles), and long$_m$ lifetime (crosses) pools are plotted as a function of the matrix [NADH], assuming 3.4 mM in the fully reduced state. Solid lines are fit with the equation $a(1 - e^{-[NADH]/K_D})$, where a is constant.

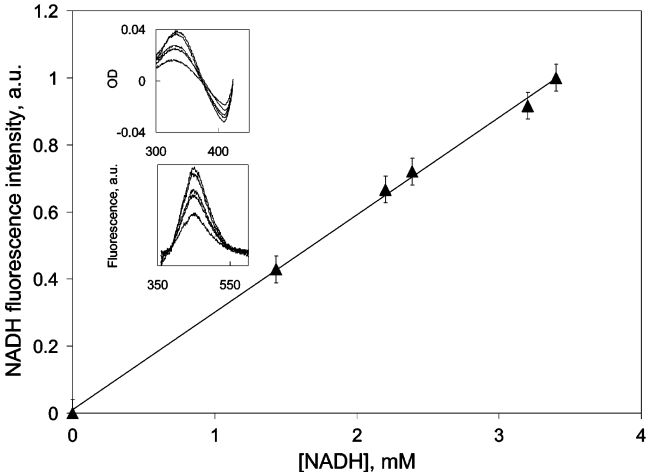

FIGURE 7: Normalized NADH fluorescence vs absorption determined matrix [NADH] in intact mitochondria. The NADH difference fluorescence and relative absorbance were measured in the same samples in 1 cm cuvettes (see Materials and Methods). The mitochondria concentration was 0.5 nmol cyt$_a$/mL. The raw fluorescence and absorbance data is presented in the two inserts of the figure. The top insert is the absorbance data; the bottom insert is the normalized fluorescence data. The NADH concentration was varied by altering the concentration of glutamate and malate in the mitochondrial suspension. [NADH] was calculated assuming 3.4 mM NADH in the matrix under fully reduced conditions (see Materials and Methods). The line represents a linear fit to the data (slope intercept is 0.29, $R = 0.99$). The error bars show the standard errors of mean values ($n = 3$).

NADH/NAD^+ ratio by GM is accompanied by other matrix changes that distort the lifetime profiles.

With regard to the relationship between NADH fluorescence and total [NADH] in the matrix, we addressed the issue in two ways. First, the absorbance of NADH at 340 nm was used to estimate total matrix [NADH], assuming that binding or the matrix environment had little effect on the absorbance at 340 nm. The relative NADH absorbance was then compared to the NADH fluorescence in the same sample (Figure 7). A linear relationship between NADH absorbance and fluorescence was observed, suggesting that the dependence of NADH binding on the NADH/NAD^+ ratio results

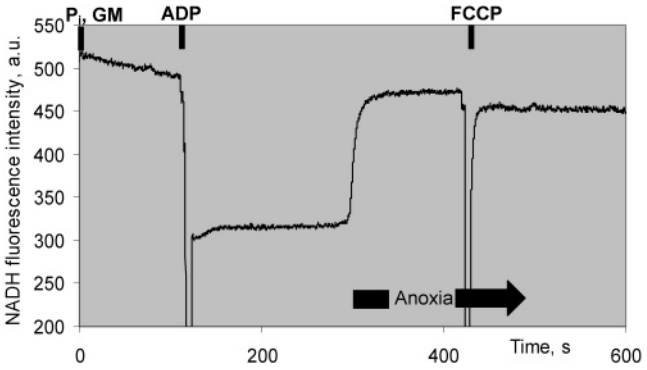

FIGURE 8: Effect of ADP and FCCP on NADH fluorescence intensity from intact heart mitochondria: [mitochondria], 1 nmol of cyt_a/mL; GM, 5 mM; P_i, 3 mM; buffer B at room temperature. The black bars represent the addition of ADP (2 mM) and FCCP (0.2 μM). Anoxia is indicated by the arrow at the bottom of the figure. Note that FCCP was added after NADH had reached its full reduction level at anoxia to evaluate the effect of uncoupler on the overall NADH emission efficiency.

in a fortuitous relationship between the amount of NADH and the emission value.

In our second approach, we modeled the lifetime data for each [NADH] and calculated the total NADH fluorescence intensity for all three pools as $\sum(\alpha_i/\alpha_{sum})\tau_i$, where $\alpha_{sum} = \alpha_{long} + \alpha_{intermediate} + \alpha_{short}$ and i represents each individual pool while α represents the relative amplitude. The NADH fluorescence intensity of fully reduced mitochondria was taken to be 1. The result of this simulation was a linear relationship ($R = 0.99$) and, within experimental error, supports the notion of a linear dependence of fluorescence intensity on total matrix [NADH]. This rather fortuitous linear relationship is due to the linear $free_m$ and $long_m$ pools and the relatively low affinity of the $intermediate_m$ pools.

One hypothesis regarding the large (~3) order of magnitude shift in the apparent NADH binding in the matrix elements between intact mitochondria and membranes could be the presence of $\Delta\Psi$ in the intact preparation. If the interaction by NADH is energetically coupled to $\Delta\Psi$, then the binding of NADH could be inhibited by $\Delta\Psi$. Indeed, taking data from Figures 4 and 6, we can estimate that only ~20% of the long lifetime sites identified in the pulverized preparation are occupied in intact mitochondria, which is consistent with this notion. This hypothesis was tested by determining the effect of dissipating $\Delta\Psi$ in intact anoxic mitochondria with an uncoupler (FCCP, 0.2 μM) on the NADH emission efficiency and on the NADH fluorescence lifetimes. If $\Delta\Psi$ was inhibiting the binding of NADH, the removal of $\Delta\Psi$ should increase the long lifetime fraction and enhance the overall fluorescence efficiency of NADH. The addition of FCCP slightly decreased the NADH fluorescence of anoxic mitochondrial NADH 3.8 ± 0.3% ($n = 3$) (Figure 8). In paired experiments, the fraction of NADH in $long_m$ was not significantly different in control (8%) and in FCCP (9%) treated samples. These data do not support the notion that $\Delta\Psi$ is inhibiting NADH binding in the mitochondrial matrix.

DISCUSSION

These data confirm the existence of different pools of NADH in the mitochondrial matrix based on their fluorescence lifetimes. From what is likely a continuum of NADH lifetimes, we found that simplifying these data by dividing them into three lifetime pools provides an effective description in concert with previous investigators (*13*). Three lifetime populations of NADH were modeled in intact mitochondria, a short lifetime pool ($free_m$: 0.4 ns), an intermediate lifetime pool ($intermediate_m$: 1.9 ns) ,and a long lifetime pool ($long_m$: 5.7 ns). Under high NADH/NAD^+ ratio conditions, the $intermediate_m$ and $long_m$ pools make up ~35% of the total NADH while contributing almost 80% of the fluorescence emission. This is due to the proportional relationship between fluorescence lifetime and intensity per molecule. Steady-state kinetic studies in intact mitochondria suggest that $long_m$ and $free_m$ were linearly dependent on the matrix [NADH]. The $intermediate_m$ reveal saturation in matrix [NADH] with a very high K_D of 2.9 mM. The matrix [NADH] dependence on binding resulted in an essentially linear relationship between total NADH fluorescence and [NADH]. Attempts to further characterize the steady-state binding kinetics of NADH in pulverized mitochondria revealed an increase in the apparent NADH affinity for binding (~20 μM) that correlates with overall NADH oxidation steady-state kinetics. The discrepancy between the affinity of NADH in pulverized mitochondria and the apparent K_Ds in the intact preparation is currently unexplained.

The largest single NADH pool in the matrix is $free_m$ at approximately two-thirds of the entire matrix NADH. This pool is consistent with a freely diffusing NADH population as characterized by the fluorescence lifetime of NADH in solution and the DAS spectral maximum. We estimate the free NADH concentration to be approximately 2.2 mM under fully reduced conditions assuming a total NADH pool of 3.4 mM (6.8 nmol/nmol of cyt_a and 2 μL matrix water/nmol of cyt_a) (*3*). This high concentration of "free" NADH contrasts with recent studies suggesting a much lower free NADH concentration in the nucleus/cytosol of ~15 mM (*35*). The apparent relationship between binding and lifetime must always be accompanied with the caveat that short-lived emission could occur from bound sites. The most obvious ways this could occur are (1) direct quenching by binding in the "folded" form (self-quenching), (2) FRET of 70−90% of the excitation to nearby absorbers such as heme, and/or (3) FRET homotransfer, first among many closely spaced bound NADH and then to a terminal free (or otherwise quenched) acceptor. In cases 1 and 2, DAS of short species would be blue shifted from free NADH, while case 3 should only occur when the bound NADH forms a proximal array with an effective concentration ≥20 mM. Interestingly, case 3 would also lead to a paradoxical rise in lifetime upon disruption/dilution, which was not observed in this study. Nevertheless, we must always consider the presence of these and other alternate lifetime modifiers when interpreting lifetime data, especially the interpretation of short lifetimes as being exclusively free. All of the spectral, lifetime, and dilution data are consistent with $free_m$ reflecting the free mobile pool of NADH in the matrix of heart mitochondria.

The two long lifetime NADH pools, $intermediate_m$ and $long_m$, are consistent with NADH populations with restricted motion thereby enhancing fluorescence emission lifetime and blue shifting the emission spectrum (see DAS spectra). These long lifetime pools had been identified by fluorescence efficiency (*6*, *7*), spectral shifts (*5*), and direct lifetime

measurements (*13*). The specific binding sites for NADH in the matrix have not been fully described. In solution, many dehydrogenases have been demonstrated to shift emission and increase emission efficiency, including malate dehydrogenase (*36*), mitochondrial aldehyde dehydrogenase (*37*), alcohol dehydrogenase (*38*−*40*), phosphoglycerate dehydrogenase (*41*), lactate dehydrogenase (*42*), and succinic semialdehyde dehydrogenase (*21*). In addition, several other enzymes and cofactors have also been demonstrated to blue shift and enhance NADH fluorescence, including citrate synthase (*22*), transcriptional cofactors (*43*), and even albumin (*7*). Thus, the immobilization of NADH leading to a blue spectral shift and extended fluorescence lifetime need not be considered as a specific interaction. However, it is also possible that NADH in a few prevalent binding sites could be the major constituents of the long lifetime NADH pools. Again, an inventory of the potential NADH binding sites in the matrix has not yet been completed. Understanding molecules involved in the immobilization of NADH would greatly aid in the understanding of the modulation of matrix NADH chemical activity as well as the mechanisms associated with the immobilization processes and control.

In intact mitochondria, NADH fluorescence intensity of $long_m$ is linear with [NADH], while the $intermediate_m$ is apparently approaching saturation with a K_D of ∼2.9 mM. These data imply that the interaction of NADH with its sites occurs well below any saturation value, resulting in a very labile NADH fluorescence signal with changes in [NADH], as has been reported in the literature for many years. Indeed, a direct comparison of NADH fluorescence with total matrix [NADH], based on 340 nm absorbance, results in an essentially linear relation (Figure 7). This relation is likely due to linear increases in $free_m$ and $long_m$ with [NADH] and the fact that $intermediate_m$ is always near its affinity value, 2.9 mM, with the limited dynamic range of matrix [NADH] (∼1−3.4 mM). The simulation of net fluorescence signal from the lifetime distributions observed as a function of [NADH] also predicts an essentially linear relation between fluorescence and [NADH], within experimental error. The linear relation between NADH fluorescence and matrix [NADH] supports the notion that NADH fluorescence is a useful method to follow the matrix NADH redox state in intact porcine heart mitochondria.

In an attempt to better characterize NADH binding kinetics, a membrane preparation was used where the matrix was essentially open. This permitted the determination of the NADH lifetime distributions and oxidation under more controlled conditions than intact mitochondria. Surprisingly, the affinity for NADH in the $intermediate_p$ and $long_p$ is much higher for binding in the disrupted membranes than in intact mitochondria, with apparent K_Ds of ∼103 and ∼24 μM, respectively. These studies on mitochondrial membranes suggest a much higher apparent affinity for NADH binding when compared to intact mitochondria (Table 2).

What could be contributing to the differences in steady-state affinity between intact mitochondria and mitochondrial membranes? Beyond the obvious differences of dilution of all matrix solutes and cofactors by >500-fold and the physical disruption of membranes in the pulverized state, $\Delta\Psi$ is completely depolarized and [NAD^+] is generally much lower in the membrane preparations where NADH is maintained in a highly reduced state. To evaluate the role of $\Delta\Psi$ in matrix NADH interactions, we repeated intact mitochondria lifetime studies in the presence of FCCP (0.2 μM) to minimize $\Delta\Psi$. In agreement with previous studies (*13*), we found no effect of FCCP on the NADH lifetime distribution or apparent fluorescence enhancement in this preparation. Thus, differences in $\Delta\Psi$ do not affect NADH binding. We could not vary the NAD^+ concentration in the pulverized preparation, since these experiments take over 15 min to run and require the presence of cyanide to maintain a steady-state [NADH] (i.e., NADH oxidation is blocked). Under these conditions, the NAD^+ is essentially in its fully reduced state; any addition of NAD^+ would simply generate more NADH through the numerous dehydrogenases. We indirectly looked for an effect of [NAD^+] on NADH binding by monitoring the effect of NAD^+ on the instantaneous rate of NADH oxidation in this preparation before significant metabolism of NAD^+ could occur. High [NAD^+] (2 mM) only shifted the half-maximal NADH oxidation concentration by 2-fold, suggesting a modest effect of NAD^+ on NADH oxidation. However, since the binding sites for NADH are unknown, we cannot eliminate a competitive inhibition of NAD^+ for NADH interaction sites not associated with NADH oxidation.

The elimination of $\Delta\Psi$ as a factor in NADH binding suggests that either the dilution or physical disruption of mitochondria might be responsible for the shift in apparent binding constant with pulverization. It has been demonstrated that complex 1 can form supramolecular complexes with matrix dehydrogenases in yeast (*44*) and in mammalian systems (*45*). These dehydrogenases include enzymes, such as malate dehydrogenase, that are known to bind NADH and cause a blue shift and enhance the fluorescence lifetime. It is possible that the disruption of mitochondria or the dilution of the matrix volume disrupts this putative complex, thus shifting the binding of NADH on these associated dehydrogenases. Evidence that the physical disruption of the mitochondria could alter dehydrogenase coupling to oxidative phosphorylation can be found in the substrate dependence of oxygen consumption in intact and pulverized mitochondria. Figure 9 presents the effects of various conditions and substrates on intact and pulverized mitochondria oxygen consumption. The cytochrome oxidase activity was evaluated using ascorbate/TMPD and found to be essentially identical in both preparations. Exogenous NADH was highly effective in supporting oxygen consumption in the pulverized preparation, in a rotenone-sensitive manner, confirming that the cytochrome chain was intact from site 1 to cytochrome oxidase. However, attempts to generate NADH with GM, or FADH with succinate, essentially result in very modest increases in oxygen consumption in the pulverized preparation in contrast to state 3 in the intact mitochondria. These data suggest that the dehydrogenases generating NADH or FADH, via GM and succinate oxidation, for the cytochrome chain are inhibited in the pulverized preparation. This could be due to the disruption of the macromolecular structures under these conditions or dilution of other critical factors with the opening of the matrix space. The hypothesis that a macromolecular complex between the dehydrogenases and complex 1 exists and influences the NADH binding and oxidation could be tested by observing the effects of generating this supramolecular complex in vitro and observing the steady-state kinetics of NADH binding and oxidation.

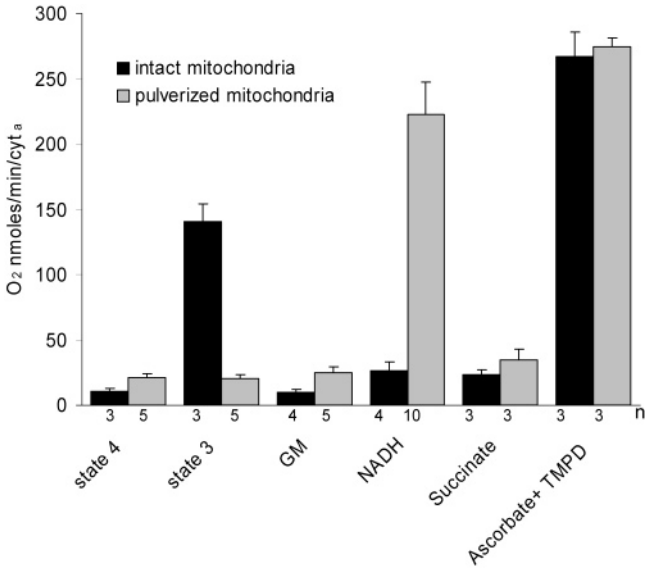

FIGURE 9: Effect of various conditions on intact and pulverized mitochondria oxygen consumption. Paired experiments were conducted to compare the ability of these preparations to consume oxygen. All experiments were conducted in buffer C at room temperature with 1 nmol of cyt_a/mL. State 4 was in the presence of 5 mM P_i and 5 mM GM. State 3 was identical to state 4 with 5 mM ADP. The GM condition was 5 mM GM alone. NADH indicated the direct addition of NADH to the bath at 1 mM. Succinate indicates the effect of adding 5 mM succinate alone. Ascorbate (2 mM) and TMPD (2 mM) were used as a control for cytochrome oxidase activity. The numbers at the bottom of each column represent the number of experiments; the error bars are the standard errors of the means.

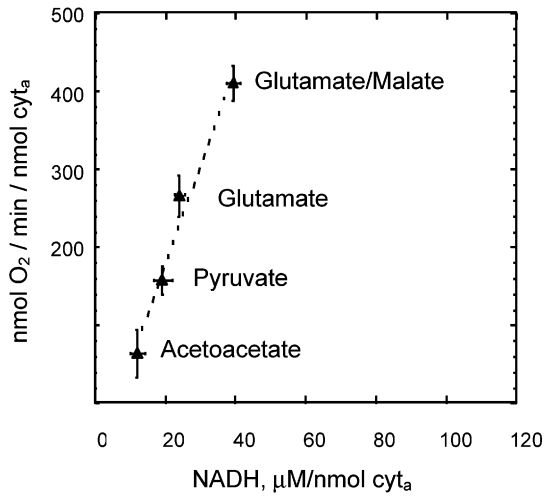

FIGURE 10: State 3 respiratory rate vs NADH fluorescence for dog heart mitochondria respiring on four different substrates. Data are from ref *46*.

How are the $intermediate_m$ and $long_m$ pools related to the oxidation of NADH by oxidative phosphorylation? In intact mitochondria, the maximum rate of oxygen consumption has been shown to be linearly related to the total NADH fluorescence in heart (*46*) and in liver (*47*, *48*) mitochondria. An example from these studies is presented in Figure 10. These data suggest that the oxidation of NADH is not saturated in the matrix under normal physiological conditions and that the affinity for NADH is much higher than the maximum ~3 mM concentration attainable in the intact matrix. Since the $intermediate_m$ and $long_m$ pools dominate the steady-state fluorescence signal, it is reasonable to suggest that the maximum rate of respiration is related to the amount of NADH in these two pools. This notion is strongly supported by observations in the pulverized preparation where the binding affinity for NADH increases by ~2 orders of magnitude in the $intermediate_p$ and $long_p$ while the half-maximal oxidation rate of NADH through the entire cytochrome chain is also shifted to essentially the same value (~20 μM). It is interesting to note that the $K_{1/2}$ for the membrane NADH oxidation is similar to the apparent affinity of isolated complex 1 for NADH (~20 μM) (*49*). On the basis of these observations, we speculate that the intermediate and long lifetime NADH pools both in intact mitochondria and in mitochondrial membranes reflect, at least partially, the NADH involved in NADH utilization by oxidative phosphorylation. The strong correlation between NADH fluorescence and mitochondrial activity state led Chance and Baltscheffsky (*8*) in 1958 to a similar conclusion suggesting the binding to "a special component of the phosphorylation system". The obvious candidate for this interaction site is complex 1 of oxidative phosphorylation, and potentially associated dehydrogenases (*50*), but (to our knowledge) no NADH fluorescence enhancement or lifetime studies on NADH binding have yet been conducted on this complex or its subunits.

In summary, three NADH fluorescence lifetime pools have been identified in intact heart mitochondria. The steady-state kinetics for the NADH interaction with these sites results in an essentially linear relationship between NADH fluorescence and matrix [NADH]. The apparent affinity of NADH is affected by the overall structure and/or concentration of cofactors in intact mitochondria, with isolated mitochondrial membranes binding and oxidizing NADH with a much higher affinity than observed in intact preparations. The specific matrix binding sites for NADH within the matrix and the membranes are unknown. However, on the basis of the tight correlation between NADH binding and the rate of oxidation, we speculate that a significant component of the NADH binding is involved in NADH oxidation by oxidative phosphorylation. The most logical location of this NADH interaction site would be within complex 1.

REFERENCES

1. Chance, B., Williamson, J. R., Famieson, D., and Schoener, B. (1965) Properties and kinetics of reduced pyridine nucleotide fluorescence of the isolated and in vivo rat heart, *Biochem. Z. 341*, 357−377.
2. Eng, J., Lynch, R. M., and Balaban, R. S. (1989) NADH fluorescence spectroscopy and imaging of isolated cardiac myocytes, *Biophys. J. 55*, 621−630.
3. Joubert, F., Fales, H. M., Wen, H., Combs, C. A., and Balaban, R. S. (2004) NADH enzyme-dependent fluorescence recovery after photobleaching (ED-FRAP): applications to enzyme and mitochondrial reaction kinetics, in vitro, *Biophys. J. 86*, 629−645.
4. Chance, B., and Thorell, B. (1959) Fluorescence measurements of mitochondrial pyridine nucleotide in aerobiosis and anaerobiosis, *Nature 184*, 931−934.
5. Chance, B., Cohen, P., Jobsis, F., and Schoener, B. (1962) Intracellular oxidation−reduction states in vivo, *Science 137*, 499−508.
6. Estabrook, R. W. (1962) Fluorometric measurements of reduced pyridine nucleotide in cellular and subcellular particles, *Anal. Biochem. 4*, 231−245.
7. Avi-Dor, Y., Olson, J. M., Doherty, M. D., and Kaplan, N. O. (1962) Fluorescence of pyridine nucleotides in mitochondria, *J. Biol. Chem. 237*, 2377−2383.

8. Chance, B., and Baltscheffsky, M. (1958) Spectroscopic effects of adenosine diphosphate upon the respiratory pigments of rat-heart-muscle sarcosomes, *Biochem. J. 68*, 283−295.
9. Chance, B., and Thorell, B. (1959) Localization and kinetics of reduced pyridine nucleotide in living cells by microfluorometry, *J. Biol. Chem. 234*, 3044−3050.
10. Thorell, B., and Chance, B. (1960) Microspectrography of respiratory enzymes within the single, mammalian cell under different metabolic conditions, *Exp. Cell Res. 20*, 43−55.
11. Nuutinen, E. M., Nishiki, K., Erecinska, M., and Wilson, D. F. (1982) Role of mitochondrial oxidative phosphorylation in regulation of coronary blood flow, *Am. J. Physiol. 243*, H159−H169.
12. Scholz, T. D., Laughlin, M. R., Balaban, R. S., Kupriyanov, V. V., and Heineman, F. W. (1995) Effect of substrate on mitochondrial NADH, cytosolic redox state, and phosphorylated compounds in isolated hearts, *Am. J. Physiol. 268*, H82−H91.
13. Wakita, M., Nishimura, G., and Tamura, M. (1995) Some characteristics of the fluorescence lifetime of reduced pyridine nucleotides in isolated mitochondria, isolated hepatocytes, and perfused rat liver in situ, *J. Biochem. (Tokyo) 118*, 1151−1160.
14. Lakowicz, J. R., Szmacinski, H., Nowaczyk, K., and Johnson, M. L. (1992) Fluorescence lifetime imaging of free and protein-bound NADH, *Proc. Natl. Acad. Sci. U.S.A 89*, 1271−1275.
15. Koretsky, A. P., and Balaban, R. S. (1987) Determination of pyridine nucleotide fluorescence from the perfused heart using an internal standard, *Am. J. Physiol. 253*, H856−H862.
16. Nuutinen, E. M. (1984) Subcellular origin of thre surface fluorescence of reduced nicotinamide nucleotides in the isolated perfused rat heart, *Basic Res. Cardiol. 79*, 131−142.
17. Patterson, G. H., Knobel, S. M., Arkhammar, P., Thastrup, O., and Piston, D. W. (2000) Separation of the glucose-stimulated cytoplasmic and mitochondrial NAD(P)H responses in pancreatic islet beta cells, *Proc. Natl. Acad. Sci. U.S.A 97*, 5203−5207.
18. Kasischke, K. A., Vishwasrao, H. D., Fisher, P. J., Zipfel, W. R., and Webb, W. W. (2004) Neural activity triggers neuronal oxidative metabolism followed by astrocytic glycolysis, *Science 305*, 99−103.
19. Koren, R., and Hammes, G. G. (1975) Interaction of reduced nicotinamide adenine dinucleotide with beef heart s-malate dehydrogenase, *Biochemistry 14*, 1021−1025.
20. Labrou, N. E., Eliopoulos, E., and Clonis, Y. D. (1996) Molecular modelling for the design of chimaeric biomimetic dye-ligands and their interaction with bovine heart mitochondrial malate dehydrogenase, *Biochem. J. 315* (Part 2), 695−703.
21. Busch, K., Piehler, J., and Fromm, H. (2000) Plant succinic semialdehyde dehydrogenase: dissection of nucleotide binding by surface plasmon resonance and fluorescence spectroscopy, *Biochemistry 39*, 10110−10117.
22. Duckworth, H. W., and Tong, E. K. (1976) The binding of reduced nicotinamide adenine dinucleotide to citrate synthase of *Escherichia coli* K12, *Biochemistry 15*, 108−114.
23. Territo, P. R., Mootha, V. K., French, S. A., and Balaban, R. S. (2000) Ca(2+) activation of heart mitochondrial oxidative phosphorylation: role of F0/F1ATPase, *Am. J. Physiol. 278*, C423−C435.
24. Balaban, R. S., Mootha, V. K., and Arai, A. (1996) Spectroscopic determination of cytochrome *c* oxidase content in tissues containing myoglobin or hemoglobin, *Anal. Biochem. 237*, 274−278.
25. Territo, P. R., and Balaban, R. S. (2000) Rapid spectrophotometric determination of oxygen consumption using hemoglobin, in vitro: light scatter correction and expanded dynamic range, *Anal. Biochem. 286*, 156−163.
26. French, S. A., Territo, P. R., and Balaban, R. S. (1998) Correction for inner filter effects in turbid samples: fluorescence assays of mitochondrial NADH, *Am. J. Physiol. 275*, C900−C909.
27. Territo, P. R., French, S. A., Dunleavy, M. C., Evans, F. J., and Balaban, R. S. (2001) Calcium activation of heart mitochondrial oxidative phosphorylation: rapid kinetics of mVO2, NADH, and light scattering, *J. Biol. Chem. 276*, 2586−2599.
28. Bose, S., French, S., Evans, F. J., Joubert, F., and Balaban, R. S. (2003) Metabolic network control of oxidative phosphorylation: multiple roles of inorganic phosphate, *J. Biol. Chem. 278*, 39155−39165.
29. Shen, F., Triezenberg, S. J., Hensley, P., Porter, D., and Knutson, J. R. (1996) Critical amino acids in the transcriptional activation domain of the herpesvirus protein VP16 are solvent-exposed in highly mobile protein segments−An intrinsic fluorescence study, *J. Biol. Chem. 271*, 4819−4826.
30. Badea, M. G., and Brand, L. (1979) Time-resolved fluorescence measurements, *Methods Enzymol. 61*, 378−425.
31. Visser, A. J. W. G., and Van Hoek, A. (1981) The fluorescence decay of reduced nicotinamides in aqueous solution after excitation with a UV−mode locked Ar ion laser, *Photochem. Photobiol. 33*, 35−40.
32. Chen, R. F., Knutson, J. R., Ziffer, H., and Porter, D. (1991) Fluorescence of tryptophan dipeptides: correlations with the rotamer model, *Biochemistry 30*, 5184−5195.
33. Knutson, J. R., Beechem, J. M., and Brand, L. (1983) Simultaneous analysis of multiple fluorescence decay curves: a global approach, *Chem. Phys. Lett. 102*, 501−507.
34. Schneckenburger, H., and Konig, K. (1992) Fluorescence decay kinetics and imaging of NAD(P)H and flavins as metabolic indicators, *Opt. Eng. 31*, 1447−1451.
35. Zhang, Q., Piston, D. W., and Goodman, R. H. (2002) Regulation of corepressor function by nuclear NADH, *Science 295*, 1895−1897.
36. Shore, J. D., Evans, S. A., Holbrook, J. J., and Parker, D. M. (1979) NADH binding to porcine mitochondrial malate dehydrogenase, *J. Biol. Chem. 254*, 9059−9062.
37. Rout, U. K., and Weiner, H. (1994) Involvement of serine 74 in the enzyme-coenzyme interaction of rat liver mitochondrial aldehyde dehydrogenase, *Biochemistry 33*, 8955−8961.
38. Chou, C. F., Lai, C. L., Chang, Y. C., Duester, G., and Yin, S. J. (2002) Kinetic mechanism of human class IV alcohol dehydrogenase functioning as retinol dehydrogenase, *J. Biol. Chem. 277*, 25209−25216.
39. Gafni, A., and Brand, L. (1976) Fluorescence decay studies of reduced nicotinamide adenine dinucleotide in solution and bound to liver alcohol dehydrogenase, *Biochemistry 15*, 3165−3171.
40. Subramanian, S., Ross, J. B., Ross, P. D., and Brand, L. (1981) Investigation of the nature of enzyme−coenzyme interactions in binary and ternary complexes of liver alcohol dehydrogenase with coenzymes, coenzyme analogues, and substrate analogues by ultraviolet absorption and phosphorescence spectroscopy, *Biochemistry 20*, 4086−4093.
41. Dubrow, R., and Pizer, L. I. (1977) Transient kinetic studies on the allosteric transition of phosphoglycerate dehydrogenase, *J. Biol. Chem. 252*, 1527−1538.
42. Stinson, R. A., and Holbrook, J. J. (1973) Equilibrium binding of nicotinamide nucleotides to lactate dehydrogenases, *Biochem. J. 131*, 719−728.
43. Fjeld, C. C., Birdsong, W. T., and Goodman, R. H. (2003) Differential binding of NAD^+ and NADH allows the transcriptional corepressor carboxyl-terminal binding protein to serve as a metabolic sensor, *Proc. Natl. Acad. Sci. U.S.A 100*, 9202−9207.
44. Grandier-Vazeille, X., Bathany, K., Chaignepain, S., Camougrand, N., Manon, S., and Schmitter, J. M. (2001) Yeast mitochondrial dehydrogenases are associated in a supramolecular complex, *Biochemistry 40*, 9758−9769.
45. Sumegi, B., and Srere, P. A. (1984) Complex I binds several mitochondrial NAD-coupled dehydrogenases, *J. Biol. Chem. 259*, 15040−15045.
46. Mootha, V. K., Arai, A. E., and Balaban, R. S. (1997) Maximum oxidative phosphorylation capacity of the mammalian heart, *Am. J. Physiol. 272*, H769−H775.
47. Moreno-Sanchez, R., Hogue, B. A., and Hansford, R. G. (1990) Influence of NAD-linked dehydrogenase activity on flux through oxidative phosphorylation, *Biochem. J. 268*, 421−428.
48. Koretsky, A. P., and Balaban, R. S. (1987) Changes in pyridine nucleotide levels alter oxygen consumption and extramitochondrial phosphates in isolated mitochondria: A ^{31}P NMR and fluorescence study, *Biochim. Biophys. Acta 893*, 398−408.
49. Fato, R., Estornell, E., Di Bernardo, S., Pallotti, F., Parenti, C. G., and Lenaz, G. (1996) Steady-state kinetics of the reduction of coenzyme Q analogs by complex I (NADH:ubiquinone oxidoreductase) in bovine heart mitochondria and submitochondrial particles, *Biochemistry 35*, 2705−2716.
50. Fukushima, T., Decker, R. V., Anderson, W. M., and Spivey, H. O. (1989) Substrate channeling of NADH and binding of dehydrogenases to complex I, *J. Biol. Chem. 264*, 16483−16488.

BI0485124